# Possible absence of a Jahn-Teller distortion critical thickness in geometrically designed LaMnO₃ films

Giovanni Annur Safarina [ORCID],[*] Yong-Jin Kim [ORCID],[*,†] and Chan-Ho Yang [ORCID][‡]

*Department of Physics and Center for Lattice Defectronics, Korea Advanced Institute of Science and Technology,*
*Daejeon 34141, Republic of Korea*

We investigated the Jahn-Teller phonon modes in LaMnO₃ film grown on an orthorhombic (110)-oriented GdScO₃ substrate using Raman spectroscopy, which enabled us to verify the presence of the cooperative Jahn-Teller distortion in the ultrathin limit. A characteristic $B_{1g}$ phonon mode with preserved symmetry was observed down to the two-unit-cell thickness. This finding suggests the absence of a film-thickness-driven critical transition of the cooperative Jahn-Teller distortion and the corresponding orbital order when the two-dimensional Jahn-Teller-distortion plane is designed to be parallel to the substrate by misfit strain.

## I. INTRODUCTION

Long-range orders associated with magnetism and ferroelectricity in reduced dimensions are usually unstable at finite temperature, according to the Mermin-Wagner theorem [1–4]. However, in magnetic systems for example, long-range ferromagnetic order in two-dimensional van der Waals crystals [5] survives due to opening a spin-wave gap by a magnetocrystalline anisotropy along with remarkable emerging functionalities [6,7]. An electrostatic counterpart, the survival of ferroelectricity at the two-dimensional limit, has been observed in ultrathin films [8,9] and monolayer membranes [10]. The discovery of enhanced ferroelectricity at the ultrathin limit [11] opens up potential applications for low-power memory devices.

Long-range ordered orbital degree of freedom, called the orbital order (OO), in strongly correlated systems mediates a variety of physical phenomena, such as transport and magnetic properties, via the concepts of double exchange or superexchange interactions [12,13]. OO has received special attention as a parent state of exotic quantum phases including high-temperature superconductivity [14,15], colossal magnetoresistance [16], and multiferroicity [17]. As observed in two-dimensional ferromagnetic and ferroelectric materials, the survival of the OO is expected to lead to exotic functional properties, opening up new applications for next-generation technologies. However, studies on the thickness dependence of the OO are highly limited [18,19].

The perovskite LaMnO₃ (space group *Pbnm*; LMO) is a canonical material for the OO of Mn $e_g$ orbitals accompanied by a cooperative Jahn-Teller (JT) distortion. In LMO,

four electrons occupy the Mn $d$ orbitals, and strong intrasite Hund's coupling causes the Mn ion to follow a high spin configuration ($t_{2g}^3 e_g^1$) [20]. MnO₆ oxygen octahedra undergo the JT distortion ($T_{JT} \sim 750$ K) [21] due to the twofold degeneracy of the Mn $e_g$ orbital, which lifts the degeneracy and lowers the electronic energy. The $d_{3x^2-r^2}/d_{3y^2-r^2}$ orbitals in the orthorhombic *ab* plane (JT plane) are alternately occupied by the cooperatively deformed oxygen ion cages created through corner sharing, as shown in Fig. 1(a) [22,23]. The superexchange interaction between the ordered intersite Mn $e_g$ electrons establishes A-type antiferromagnetic order with a Néel temperature of $T_N \sim 140$ K [20].

In our previous studies, we reported that the orientation of the JT plane could be controlled by strain engineering, and that the orientation could be determined through a resonant x-ray scattering technique [23] and Raman spectroscopy [24,25]. The existence of a critical thickness was elucidated when the JT plane was perpendicular to the substrate surface; in this condition, the thickness is a control parameter of dimensionality, from two-dimensional planes toward quasi-one-dimensional nanostrips [19]. The OO and JT distortion were suppressed below this threshold, and the orbital occupancy became more isotropic. This leads us to consider the existence of a critical thickness in a system with the JT plane aligned parallel to the substrate, and how the characteristic phonons of the system appear in the ultrathin film regime.

## II. GROWTH AND CHARACTERIZATION

We prepared epitaxial LMO thin films on GdScO₃ (GSO) substrates using pulsed laser deposition equipped with a KrF excimer laser (248 nm in wavelength). The GSO substrate provides an appropriate interface because of the absence of a JT distortion [26] and the exclusion of the polar discontinuity problem [27,28]. The LMO films were grown at a substrate temperature of 900 °C in a 9:1 gas combination of Ar and O₂ at 0.1 Torr. To eliminate excess oxygen and fix

_____

[*]These authors contributed equally to this work.

[†]Author to whom correspondence should be addressed: neutronk@kaist.ac.kr

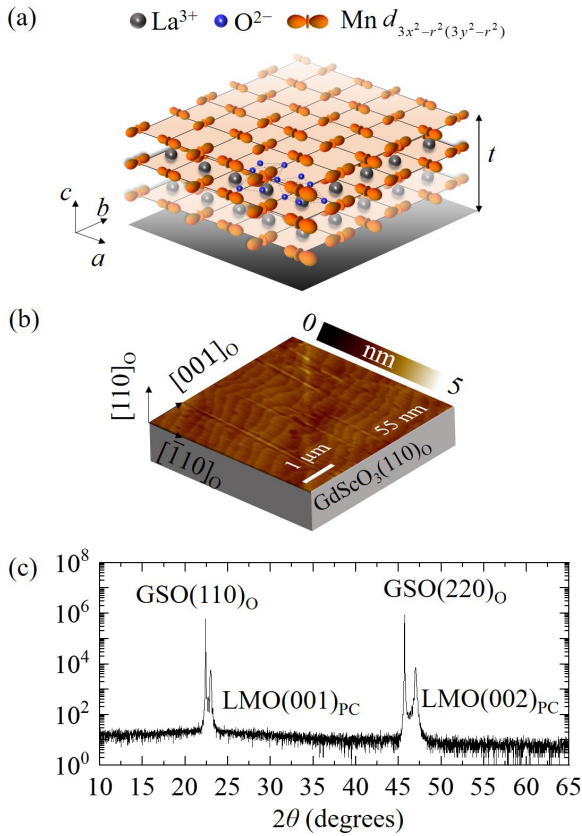[‡]Author to whom correspondence should be addressed: chyang@kaist.ac.kr

FIG. 1. (a) Schematic diagram of a cooperative JT distortion and the resultant OO of occupied Mn orbitals. The light-pink plane indicates the JT plane, corresponding to the *ab* plane. The control parameter "*t*" represents the thicknesses of the films. (b) A surface topographic image of a 55-nm-thick LMO thin film grown on GSO substrate. (c) An x-ray $\theta - 2\theta$ scan, including LMO $(001)_{PC}$ and LMO $(002)_{PC}$ peaks. Here, the subscripts "$_O$" and "$_{PC}$" represent the orthorhombic and pseudocubic indices, respectively.



FIG. 2. Surface topographic images of ultrathin films of LMO on GSO substrate. The scan size is 2.5 μm × 5 μm.

the cation vacancy issue, the sample was cooled down to an ambient temperature at a rate of 10 °C min$^{-1}$ in vacuum condition ($\sim 10^{-6}$ Torr). The surface topographies of the films were characterized using an atomic force microscope (Bruker Multimode V equipped with a nanoscope controller V) with Si tips (HQ:NSC35, MikroMasch). Figure 1(b) shows the surface topographic image of a 55-nm-thick LMO thin film grown on the GSO substrate.

To analyze the crystal structure of the epitaxial thin film, x-ray diffraction data including a conventional $\theta - 2\theta$ scan was taken using an x-ray diffractometer (PANalytical X'pert-PRO MRD) with Cu $K\alpha_1$ radiation ($\lambda = 1.5406$ Å). Figure 1(c) exhibits an x-ray $\theta - 2\theta$ scan, including the LMO $(001)_{PC}$ and $(002)_{PC}$ peaks. In a wide range of scan angle, only the LMO film and substrate peaks were detected, indicating that our film had good quality without impurity phase. From the $\theta - 2\theta$ scan, the out-of-plane lattice parameter of the LMO film was estimated to be 3.86 Å, which is similar to the *c*-axis lattice parameter of bulk LMO in terms of a pseudocubic unit cell. This suggests that the orientation of the JT plane in our film is parallel to the substrate surface.
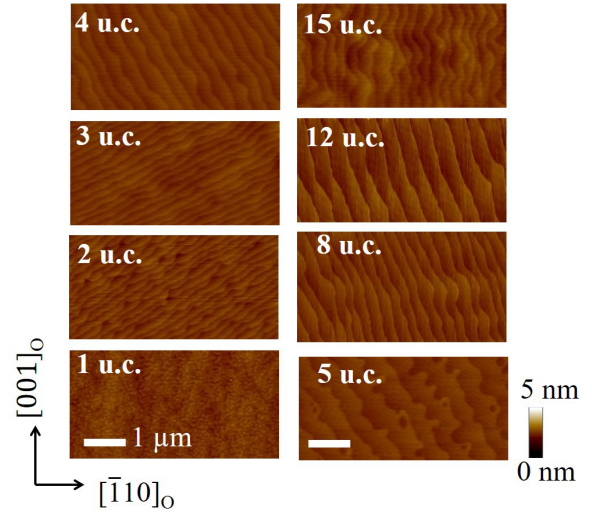
Then, a series of high-quality LMO ultrathin films were prepared with thicknesses of 1–15 unit cells (u.c.) on GSO substrates. To control the film thickness, we referred to the thick sample of LMO and estimated the number of ablated laser pulses needed for every unit cell. The surface topographic images of the ultrathin film LMO/GSO are shown in Fig. 2. Atomically flat surfaces were observed with a step-terrace structure for all ultrathin film samples, except for the one-u.c. sample, indicating there was a step-flow growth mode during the high-temperature LMO deposition. Because the nominally one-u.c. sample had an untidy terrace structure with incomplete coverage, investigation of the thickness effect was conducted down to a two-u.c. film.

## III. RAMAN SPECTROSCOPY

### A. Raman spectroscopy of thin films

To determine the existence and the orientation of the JT plane in the LMO/GSO system, we investigated the symmetry of JT phonon modes in the films using confocal Raman spectroscopy at room temperature. Raman spectra were obtained using a confocal Raman spectroscope alpha 300R (WITec GmbH, Germany). The Raman spectra were excited using a Nd:YAG 532-nm laser, and were recorded in backscattering geometry using a UHTS 600 spectrometer. A laser power density of $\sim 20$ kW/mm$^2$ at the sample surface was used.

In bulk LMO, there are 24 Raman-active modes ($7A_g + 7B_{1g} + 5B_{2g} + 5B_{3g}$ in the *Pbnm* notation) among the total 60 $\Gamma$-point phonons [29]. Based on the lattice dynamic calculation, the phonon with $B_{1g}$ ($A_g$) symmetry near $\sim 615$ cm$^{-1}$ ($\sim 490$ cm$^{-1}$) corresponds to the in-phase (out-of-phase) vibration of oxygens in the JT plane. The $A_g$ mode originates from the JT distortion and octahedral rotation, and the $B_{1g}$ mode originates from the pure JT distortion.

In this work, we define polarization directions *x* and *y* as the $[1\bar{1}0]_O$ and $[001]_O$ directions of the substrate (here, the subscript "$_O$" represents orthorhombic indices), which
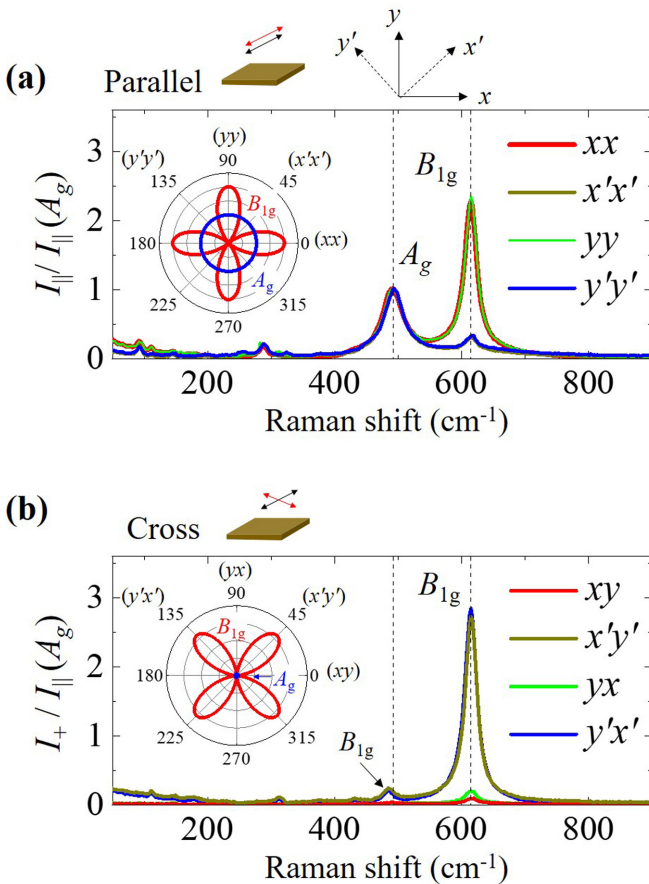
FIG. 3. Polarized Raman spectra of a 55-nm-thick LMO film grown on GSO. (a) The Raman spectra measured in a parallel-polarization geometry. The inset figure indicates the polar plots of the $A_g$ (blue) and $B_{1g}$ (red) intensities for the parallel-polarization geometry. (b) The Raman spectra measured in a cross-polarization geometry. The inset figure indicates the polar plots of the $A_g$ (blue) and $B_{1g}$ (red) intensities for the cross-polarization geometry. The vertical dashed lines correspond to the $A_g$ mode at $\sim 490$ cm$^{-1}$ and the $B_{1g}$ mode at $\sim 615$ cm$^{-1}$. All the spectra were normalized by the intensity of the $A_g$ peak.

correspond to two peudocubic axes of the perovskite unit cell. Polarization-dependent Raman spectra of the 55-nm-thick LMO/GSO sample were measured at eight different polarization configurations, including $(xx)$, $(yy)$, $(x'x')$, and $(y'y')$ for the parallel-polarization geometry and $(xy)$, $(yx)$, $(x'y')$, and $(y'x')$ for the cross-polarization geometry. The first (final) symbol represents the linear light polarization of incident (scattered) light. The orientation of each axis within the plane parallel to substrate is displayed in Fig. 3.

Using the Raman tensor analysis for the bulk LMO, we can calculate the light-polarization dependence of the JT phonon modes [23]. When the JT plane is parallel to the substrate, and the light polarizations are in that plane and parallel to each other, a fourfold symmetry of the $B_{1g}$ mode intensity is expected peaking for polarization parallel to the $x$ and $y$ axes. On the other hand, the intensity of the $A_g$ mode is polarization independent [see the inset of Fig. 3(a)]. In the cross-polarization geometry, the $B_{1g}$ mode has fourfold sym-

metry with maximum intensity in the diagonal directions, and the intensity of the $A_g$ mode vanishes [see inset of Fig. 3(b)]. Therefore, both the $A_g$ and the $B_{1g}$ phonon modes are allowed in the $(xx)$ and $(yy)$ polarization geometries while only the $A_g$ phonon mode is allowed in the $(x'x')$ and $(y'y')$ geometries.

The experimental results showed good agreement with the expected symmetry properties in the Raman spectra. For a quantitative comparison, the spectra were normalized by the intensities of the $A_g$ mode measured in the parallel polarizations. We measured Raman spectra in a parallel configuration first, and then obtained the cross-polarization data by changing the analyzer by 90° without changing the sample orientation or position. For example, we first got the data at $(xx)$ and then subsequently at $(xy)$ without touching the sample. Accordingly, the experimental error could be reduced by normalizing the $A_g$ mode measured in the parallel-polarization configuration.

As shown in Fig. 3(a), the Raman intensity of the $B_{1g}$ mode was at its highest when the light polarization was parallel to the $x$ and $y$ (or [1$\bar{1}$0]$_O$ and [001]$_O$ directions), such as $(xx)$ and $(yy)$, while the intensity was significantly suppressed when the light polarization was in the diagonal directions, $(x'x')$ and $(y'y')$. The residual peaks at $\sim 615$ cm$^{-1}$ at $(x'x')$ and $(y'y')$ could be ascribed to the minor involvement of the cross-polarization component by a marginal misalignment between the polarizations of the incident and scattered light. The estimated polarization leakage defined as the ratio of the average intensity of $(x'x')$ and $(y'y')$ and the average intensity of $(xx)$ and $(yy)$ was 14%.

In the cross-polarization geometry, the $A_g$ mode's intensity almost vanished for all polarization configurations, as shown in Fig. 3(b). In addition, the Raman intensity of the $B_{1g}$ mode at $\sim 615$ cm$^{-1}$ was maximum when the light polarization was in the diagonal directions, $(x'y')$ and $(y'x')$, while the $B_{1g}$ mode's intensity was largely reduced when the light polarization was in on-axis $(xy)$ and $(yx)$ polarization geometries. Additional $B_{1g}$ modes at $\sim 485$ cm$^{-1}$ were observed and corresponded to the scissors-like vibration of the basal oxygens in the JT plane [29]. The residual peaks at $\sim 615$ cm$^{-1}$ at $(xy)$ and $(yx)$ were ascribed to involvement of the parallel-polarization component. The symmetry analysis of the phonon modes suggests that the orientation of the JT plane in the LMO thin film was parallel to the GSO substrate. These results are consistent with our previous study of resonant x-ray scattering experiments [23].

Next, we obtained the thickness-dependent polarized Raman spectra of the $(x'y')$ polarization geometry to selectively investigate the $B_{1g}$ mode, as shown in Fig. 4(a). The $B_{1g}$ mode originates from the pure JT distortion and is important for characterizing the JT distortion. As shown in Fig. 4(a), the intensity of the $B_{1g}$ mode gradually weakened and widened as the thickness was reduced. The $B_{1g}$ mode was still detected in the two-u.c. thickness sample.

Each Raman spectrum was fitted to a Lorentzian model to obtain detailed information about the Raman shift, spectra width, and spectra area. As displayed in Fig. 4(b), the Raman shift of the $B_{1g}$ mode was around 615–617 cm$^{-1}$ in the thick regime of the films. A noticeable Raman shift toward higher wave number was observed in the ultrathin limit, thinner than five-u.c.-thick films. The hardening of the $B_{1g}$ mode indicates
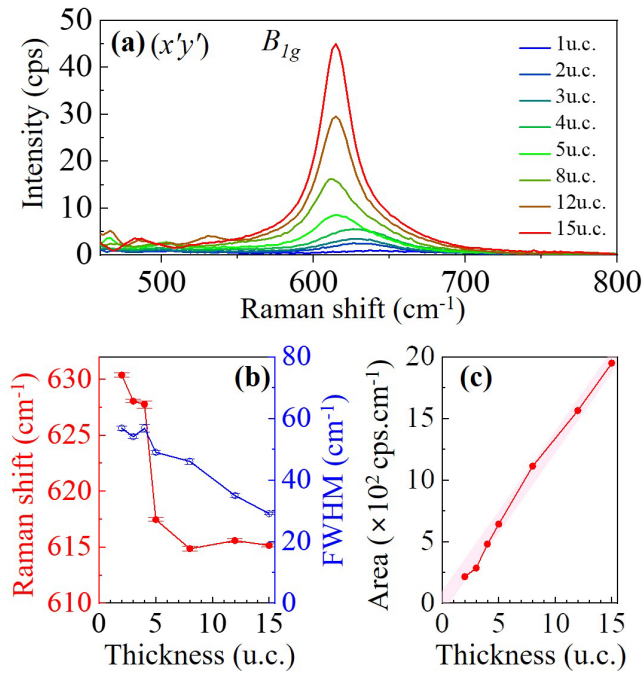
FIG. 4. Thickness dependence of (a) polarized Raman spectra of the $B_{1g}$ mode measured in the $(x'y')$ polarization geometry. Corresponding (b) Raman shift (red) and spectra width (blue), and (c) spectral areas of the LMO/GSO thin films.

that these ultrathin films have stronger strain and/or symmetry mismatch effects comparing to the films thicker than five u.c. thickness. In addition, the spectral width of the $B_{1g}$ mode gradually broadened as the thickness decreased, indicating higher instability of the JT phonons in the ultrathin film limit. Furthermore, according to Fig. 4(c), the spectral area shows a gradual decrease as the thickness is reduced. The continuous linear relationship between the area and thickness down to two u.c. film indicates the JT distortion has a stable order parameter, based on the proportionality of Raman intensity to film thickness [30].

### B. Angle-resolved Raman spectroscopy

After we observed the hardening of the original $B_{1g}$ mode, we reexamined the symmetry of the phonon to be more confident about the possible absence of a critical thickness, using angle-resolved Raman spectroscopy for two-u.c.-thick film. In this case, the angle $(\varphi)$ of normal-incident light polarization spans from the $x$ direction. Figure 5(a) depicts the angle-resolved Raman intensity of the two-u.c.-thick film. The Raman intensity of the $B_{1g}$ mode in the parallel-polarization geometry was maximized when the light polarization was parallel to the $x(= 0°, 180°)$ and $y(= 90°, 270°)$ directions, while it was greatly suppressed when the light polarization was in the diagonal directions, i.e., $= 45°, 135°, 225°, 315°$.

To clearly determine the symmetry of the $B_{1g}$ mode, we plotted the polarization angle-dependent Raman intensity, as shown in Fig. 5(b). The experimental data for the $B_{1g}$ mode intensity shows a clear four-lobed structure which is well matched with the simulation result (a solid four lobed) as shown in Fig. 3(b). This kind of Raman intensity changes
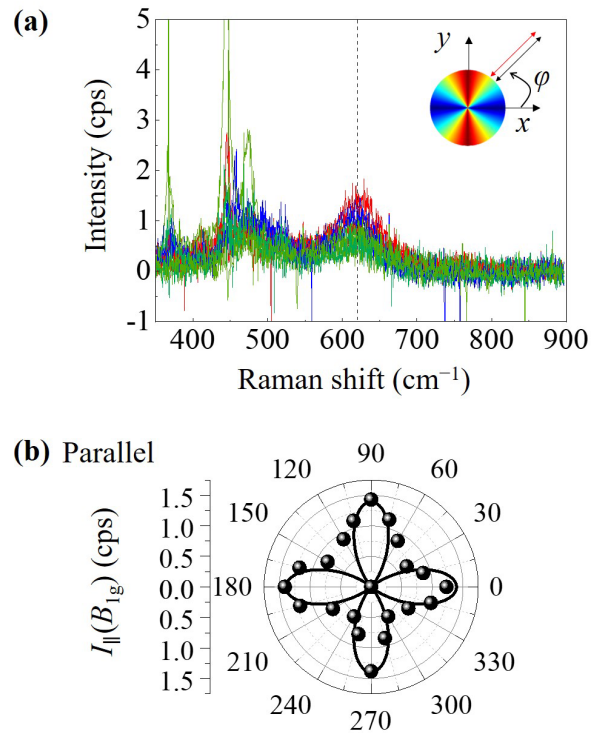


FIG. 5. (a) Angle-resolved Raman spectra of a two-u.c.-thick film measured in the parallel-polarization geometry. (b) The corresponding polar plots of the $B_{1g}$ mode intensity in the parallel-polarization geometry. The solid line corresponds to the simulation result and the black circle indicates the experimental data.

follow the Raman spectra selection rule for the parallel JT plane configuration to the substrate, as observed in the thick regime. This finding suggests the JT distortion exists down to two u.c. thickness in terms of phonon symmetry, and the possible absence of a critical thickness for the cooperative JT distortion and corresponding OO when the JT plane is placed parallel to the substrate.

This finding is in contrast with the LMO/DyScO$_3$ system, where a critical thickness exists when the JT plane is perpendicular to the substrate. This implies that the reduction of the edge-to-interior ratio within the JT plane enhances the instability of the cooperative JT distortion and the OO more severely than the simple reduction of the stacking number of the JT planes. Therefore, tailoring the crystallographic orientation will be a key factor in determining the existence or absence of a critical thickness of the conjugate OO in thin films.

### IV. CONCLUSION

In this study, we investigated the critical thickness of a JT distortion when the JT plane is parallel to the substrate. We designed the JT plane of LMO to be parallel to the substrate using a GSO substrate and confirmed it by symmetry analysis of the JT phonons. With the given geometry, we selectively measured the pure JT-originated $B_{1g}$ mode in a series of thin films with various thicknesses. We observed a continuous linear relation between the thickness and Raman intensity, and based on this the possible absence of a critical thickness of

JT distortion was presumed. We reevaluated the symmetry of the $B_{1g}$ phonon mode for a two-u.c.-thick film, which showed the same symmetry as the thick film, suggesting the survival of the JT distortion and OO in the ultrathin limit. Our study reveals that the orientation of the two-dimensional JT plane with respect to the substrate plays a key role in stabilizing low-dimensional OO systems.

[1] N. D. Mermin and H. Wagner, Absence of Ferromagnetism or Antiferromagnetism in One- or Two-Dimensional Isotropic Heisenberg Models, Phys. Rev. Lett. **17**, 1133 (1966).

[2] F. Liu, S. N. Khanna, and P. Jena, Quantum size effect on the magnetism of finite systems, Phys. Rev. B **42**, 976 (1990).

[3] J. E. Rault, W. Ren, S. Prosandeev, S. Lisenkov, D. Sando, S. Fusil, M. Bibes, A. Barthélémy, L. Bellaiche, and N. Barrett, Thickness-Dependent Polarization of Strained BiFeO$_3$ Films with Constant Tetragonality, Phys. Rev. Lett. **109**, 267601 (2012).

[4] N. A. Spaldin, Fundamental size limits in ferroelectricity, Science **304**, 1606 (2004).

[5] C. Gong, L. Li, Z. Li, H. Ji, A. Stern, Y. Xia, T. Cao, W. Bao, C. Wang, Y. Wang *et al.*, Discovery of intrinsic ferromagnetism in two-dimensional van der Waals crystals, Nature (London) **546**, 265 (2017).

[6] M. Gibertini, M. Koperski, A. F. Morpurgo, and K. S. Novoselov, Magnetic 2D materials and heterostructures, Nat. Nanotechnol. **14**, 408 (2019).

[7] Y. Liu, N. O. Weiss, X. Duan, H.-C. Cheng, Y. Huang, and X. Duan, Van der Waals heterostructures and devices, Nat. Rev. Mater. **1**, 16042 (2016).

[8] P. Gao, Z. Zhang, M. Li, R. Ishikawa, B. Feng, H.-J. Liu, Y.-L. Huang, N. Shibata, X. Ma, S. Chen *et al.*, Possible absence of critical thickness and size effect in ultrathin perovskite ferroelectric films, Nat. Commun. **8**, 15549 (2017).

[9] H. Wang, Z. R. Liu, H. Y. Yoong, T. R. Paudel, J. X. Xiao, R. Guo, W. N. Lin, P. Yang, J. Wang, G. M. Chow *et al.*, Direct observation of room-temperature out-of-plane ferroelectricity and tunneling electroresistance at the two-dimensional limit, Nat. Commun. **9**, 3319 (2018).

[10] D. Ji, S. Cai, T. R. Paudel, H. Sun, C. Zhang, L. Han, Y. Wei, Y. Zang, M. Gu, Y. Zhang *et al.*, Freestanding crystalline oxide perovskites down to the monolayer limit, Nature (London) **570**, 87 (2019).

[11] S. S. Cheema, D. Kwon, N. Shanker, R. dos Reis, S.-L. Hsu, J. Xiao, H. Zhang, R. Wagner, A. Datar, M. R. McCarter *et al.*, Enhanced ferroelectricity in ultrathin films grown directly on silicon, Nature (London) **580**, 478 (2020).

[12] M. B. Salamon and M. Jaime, The physics of manganites: Structure and transport, Rev. Mod. Phys. **73**, 583 (2001).

[13] K. I. Kugel and D. I. Khomskiĭ, The Jahn-Teller effect and magnetism: Transition metal compounds, Sov. Phys. Usp. **25**, 231 (1982).

[14] P. A. Lee, N. Nagaosa, and X.-G. Wen, Doping a Mott insulator: Physics of high-temperature superconductivity, Rev. Mod. Phys. **78**, 17 (2006).

[15] H.-B. Jang, J. S. Lim, and C.-H. Yang, Film-thickness-driven superconductor to insulator transition in cuprate superconductors, Sci. Rep. **10**, 3236 (2020).

[16] S. Jin, T. H. Tiefel, M. McCormack, R. A. Fastnacht, R. Ramesh, and L. H. Chen, Thousandfold change in resistivity in magnetoresistive La-Ca-Mn-O films, Science **264**, 413 (1994).

[17] K. Singh, C. Simon, E. Cannuccia, M.-B. Lepetit, B. Corraze, E. Janod, and L. Cario, Orbital-Ordering-Driven Multiferroicity and Magnetoelectric Coupling in GeV$_4$S$_8$, Phys. Rev. Lett. **113**, 137602 (2014).

[18] M. Huijben, L. W. Martin, Y.-H. Chu, M. B. Holcomb, P. Yu, G. Rijnders, D. H. A. Blank, and R. Ramesh, Critical thickness and orbital ordering in ultrathin La$_{0.7}$Sr$_{0.3}$MnO$_3$ films, Phys. Rev. B **78**, 094413 (2008).

[19] Y.-J. Kim, C. Lee, H.-S. Park, Y. Yeo, G. A. Safarina, D. D. Le, J.-G. Kim, D. Bang, B.-G. Cho, J.-H. Park *et al.*, Orbital order melting at reduced dimensions, Nano Lett. **22**, 1059 (2022).

[20] C. Ritter, M. R. Ibarra, J. M. De Teresa, P. A. Algarabel, C. Marquina, J. Blasco, J. García, S. Oseroff, and S-W. Cheong, Influence of oxygen content on the structural, magnetotransport, and magnetic properties of La Mn O$_{3+\delta}$, Phys. Rev. B **56**, 8902 (1997).

[21] J. Rodríguez-Carvajal, M. Hennion, F. Moussa, A. H. Moudden, L. Pinsard, and A. Revcolevschi, Neutron-diffraction study of the Jahn-Teller transition in stoichiometric LaMnO$_3$, Phys. Rev. B **57**, R3189(R) (1998).

[22] Y. Murakami, J. P. Hill, D. Gibbs, M. Blume, I. Koyama, M. Tanaka, H. Kawata, T. Arima, Y. Tokura, K. Hirota *et al.*, Resonant X-Ray Scattering from Orbital Ordering in LaMnO$_3$, Phys. Rev. Lett. **81**, 582 (1998).

[23] Y.-J. Kim, J. H. Lee, S.-W. Kim, T. Y. Koo, and C.-H. Yang, Orientation control of the orbital ordering plane in epitaxial LaMnO$_3$ thin films by misfit strain, Europhys. Lett. **116**, 27003 (2016).

[24] Y.-J. Kim, H.-S. Park, and C.-H. Yang, Raman imaging of ferroelastically configurable Jahn–Teller domains in LaMnO$_3$, npj Quantum Mater. **6**, 62 (2021).

[25] G. A. Safarina, Y.-J. Kim, H.-S. Park, and C.-H. Yang, Raman spectroscopy of the Jahn–Teller phonons in a magnetic LaMnO$_3$ thin film grown on KTaO$_3$, J. Appl. Phys. **131**, 025302 (2022).

[26] R. P. Liferovich and R. H. Mitchell, A structural study of ternary lanthanide orthoscandate perovskites, J. Solid State Chem. **177**, 2188 (2004).

[27] Z. Chen, Z. Chen, Z. Q. Liu, M. E. Holtz, C. J. Li, X. R. Wang, W. M. Lü, M. Motapothula, L. S. Fan, J. A. Turcaud *et al.*, Electron Accumulation and Emergent Magnetism in LaMnO$_3$/SrTiO$_3$ Heterostructures, Phys. Rev. Lett. **119**, 156801 (2017).

[28] X. R. Wang, C. J. Li, W. M. Lü, T. R. Paudel, D. P. Leusink, M. Hoek, N. Poccia, A. Vailionis, T. Venkatesan, J. M. D. Coey *et al.*, Imaging and control of ferromagnetism in LaMnO$_3$/SrTiO$_3$ heterostructures, Science **349**, 716 (2015).

[29] M. N. Iliev, M. V. Abrashev, J. Laverdière, S. Jandl, M. M. Gospodinov, Y.-Q. Wang, and Y.-Y. Sun, Distortion-dependent Raman spectra and mode mixing in $R$MnO$_3$ pervoskites ($R$ = La, Pr, Nd, Sm, Eu, Gd, Tb, Dy, Ho, Y), Phys. Rev. B **73**, 064302 (2006).

[30] H. G. Lee, R. Kim, J. Kim, M. Kim, T. H. Kim, S. Lee, and T. W. Noh, Anisotropic suppression of octahedral breathing distortion with the fully strained BaBiO$_3$/BaCeO$_3$ heterointerface, APL Mater. **6**, 016107 (2018).